Paleogene Initiation of the Western Branch of the East African Rift: the uplift history of the Rwenzori Mountains, Western Uganda

Scott Jess[1*], Daniel Koehn[2], Matthew Fox[3], Eva Enkelmann[1], Till Sachau[4] and Kevin Aanyu[5]

[1] University of Calgary, Department of Geoscience, Calgary, Alberta T2N 1N4, Canada.

[2] Geo-Zrntrum Nordbayern, University Erlangen-Nuremberg, Erlangen, Germany.

[3] Department of Earth Sciences, University College London, London, UK.

[4] Department of Geosciences, Eberhard Karls University Tübingen, Tübingen, Germany.

[5] Department of Geology and Petroleum Studies, College of Natural Sciences, Makerere University, P.O. Box 7062, Kampala, Uganda

*corresponding author: scott.jess@ucalgary.ca

Abstract

The two branches of the East African Rift System (EARS) are believed to have initiated diachronously. However, a growing body of work continues to suggest the onset of rifting in the Western Branch occurred in the Palaeogene, coeval to the Eastern Branch. Due to a lack of pre-Miocene stratigraphy, attempts to resolve the geological history of the Western Branch must study the uplift and erosional histories of the modern rift topography. In this study, the rock uplift history of the Rwenzori Mountains, Western Uganda, is resolved to better our understanding of the tectonic history of the Western Branch of the EAR. Through the application of low-temperature thermochronology, χ-mapping and the modelling of river profiles, we show that rock uplift of the Rwenzori dates back to the Oligocene, with thermal history models suggesting uplift induced exhumation may date back as far as the Eocene. This provides tangible evidence that extension began in the region in the Paleogene, coeval with the Eastern Branch, and not the late Neogene. These results have broad implications for the tectonic evolution of the entire East African Rift System and suggest our current understanding of the region's rift history remains incomplete.

Keywords: East African Rift, Western Branch, Rifting, Thermochronology, Uplift, River Profile

1 Introduction

Continental rifts are a crucial feature of plate tectonic theory and are fundamental in understanding the history of the earth's crust (Bosworth, 1985; Rosendahl, 1987; Olsen & Morgan, 2006; Misra & Mukherjee, 2015). The East African Rift System (EARS) is a definitive example of a continental rift system (Fig. 1), allowing us to closely examine numerous features found within active rift settings (Ebinger, 1989; Morley & Ngenoh, 1999; Chorowicz, 2005; Stamps et al., 2008). The EARS is separated into two branches that are believed to have formed diachronously, the Eastern Branch in the Eocene (~40 Ma) and the Western Branch in the Miocene (~12 Ma), though it has been postulated that rifting in the western branch may also date back to the Paleogene (Roberts et al., 2012). Palaeogene stratigraphy in the Western Branch is very limited, especially in northern sectors, hence characterizing the tectonic history prior to the Miocene requires study of the rift related topography.

The Rwenzori Mountains, Western Uganda, are the world's highest rift mountains (max elevation 5,109 m) and are widely considered to represent an uplifted horst block within the northern Western Branch of the EARS (Fig. 1) (Bauer et al., 2010). Biostratigraphic and stratigraphic analysis from surrounding syn-rift sediments has previously been used to infer the Rwenzori were low lying during much of the Miocene, overlain by a vast paleo-lake (Obweruka) (Pickford et al., 1992; Schneider et al., 2016) and experienced significant rock uplift during the late Miocene-Pliocene at an estimated rate of ~1.6 km/Myr (MacPhee, 2006). Although previous thermochronometric studies from the Rwenzori basement have supported this estimate, they failed to effectively resolve the Neogene and Quaternary history (Roller et al., 2012; Bauer et al., 2013).

Tectonic mechanisms that are used to explain the rapid rise of the Rwenzori include rift interaction, isostatic forces or crustal delamination as possible drivers for uplift (Ring, 2008; Wallner & Schmeling, 2010). Initial models predicted the coupling of stress reorientation and glacial erosion may have started dramatically unroofing the crust ~2.3 Ma (Ring, 2008), while others suggest delamination of the lower crust following the interaction of two propagating rift systems led to rapid uplift over a period of only 1.2 Myrs (Wallner & Schmeling, 2010). These proposed mechanisms deviate from traditional extensional tectonics and suggest either the Rwenzori are a highly unique tectonic feature or that our understanding of the tectonic history is incomplete and further studies are required. In this study, we aim to constrain the rock uplift history of the Rwenzori Mountains using new low-temperature thermochronological data, χ-mapping and river profile models that together quantify the rate of rock uplift across the region and help to address how the topography of the Rwenzori formed. These results help to better resolve the tectonic history of the region and provide greater insight into broader rifting history of the EARS.

2 Geological background

The underlying basement of the Rwenzori is a combination of Archaean gneisses and Proterozoic schists and amphibolites of the Buganda-Toro fold and thrust belt (Koehn et al., 2016). The belt comprises thick-skinned nappes of Archean gneiss, Paleoproterozoic metasediments and orthogneiss, thrusted together during mid-Paleozoic collision (Link et al., 2010) (Fig. 2). Fabrics within this metamorphic basement do show similarities to the orientation of rift propagation within the region, consistent with the belief the Western Branch of the EARS follows a trend of Proterozoic fold and thrust belts situated between the Tanzania and Congo cratons (Link et al., 2010) (Fig. 1).

Extension of the continental crust across Eastern Africa began in the Paleogene and created two divisions of rifting, the Eastern and Western branches (Morley & Ngenoh, 1999). The onset of extension across the Eastern Branch dates back to the Eocene, constrained by the timing of volcanism in the region and rift related stratigraphy (Ebinger et al., 1989; Morley et al., 1992; Mcdougall & Brown, 2009). The Western branch of the EARS is thought to have begun developing much later, in the Miocene (Morley & Ngenoh, 1999), though reviews of stratigraphy, volcanic geochronology and low-temperature thermochronology have suggested the timing of rift initiation may be drawn back to the Oligocene (Roberts et al., 2012; Mortimer et al., 2016). The lack of well exposed pre-Miocene sediment across the region makes it difficult to effectively date the timing of rift initiation, though it has been suggested that the region underwent uplift in the Eocene (van der Beek, 1998).

Miocene extension of the Western Branch of the EARS is believed to have initiated rock uplift of the Rwenzori. Biostratigraphy analysis of sediment from the Kisegi-Nyabusosi area suggests the region was covered by a single large palaeo-lake in the Miocene (Lake Obweruka), implying the topography of the Rwenzori was absent (Pickford et al., 1992). This is supported by petrological analysis of sediments north of the Rwenzori showing a significant change in mineral assemblage at the Miocene/Pliocene boundary (~5.5 - 5.0 Ma), suggesting uplift of the Rwenzori began at this time (Schneider et al., 2016). Previous thermochronological studies in the region support this interpretation, suggesting that rapid rock uplift occurred during the Pliocene-Pleistocene and erosion has failed to keep up, leading to dramatic surface uplift (Bauer et al., 2010; Bauer et al., 2012; Bauer et al., 2013). This lack of erosion has resulted in Oligocene and older apatite fission-track and (U-Th)/He ages (Bauer et al., 2010; Bauer et al., 2012; Bauer et al., 2013). Though thermal history modelling of the data is consistent with rapid cooling through the Neogene and Quaternary (Bauer et al., 2010; Bauer et al., 2012; Bauer et al., 2013), previous work has highlighted how thermochronological data fails to effectively resolve this period due to a lack of erosion-driven cooling (MacPhee, 2006) and a direct rate of exhumation cannot by extracted. Additionally, heavy vegetation cover makes it challenging to map extensional and compressional structures across the Rwenzori and many features are inferred from geomorphology and contrasting thermochronological ages (Bauer et al., 2013), making it difficult to corroborate interpretations with observable geology.

3 Methodology

3.1 Apatite low-temperature thermochronology

This study utilizes apatite fission-track (AFT) and (U-Th)/He analysis (AHe) to resolve a given rock sample's thermal history. Each method provides temporal information from a defined temperature window: the AFT partial annealing zone (PAZ; 120 °C – 60 °C; Gallagher et al., 1998) and the AHe partial retention zone (HePRZ; ~70 °C – 40 °C; Gautheron et al., 2012). The thermal sensitivity of each system depends on many factors including grain chemistry, thermal history, grain size, geometry and degree of radiation damage, which influence fission-track annealing and helium diffusion kinetics (Ketcham et al., 2007; Gautheron et al., 2012). These controls on annealing and diffusion generally lead to a range of ages being derived from a rock sample, a feature that can be utilised within thermal history modelling (Ketcham et al., 2007). However, other factors can also influence a grain's age that are difficult to account for within the modelling process; such as implantation, mineral inclusions and isotope zonation (Wildman et al., 2016 and references therein), meaning ages cannot always be effectively modelled. Bedrock samples from 12 locations were analysed as part of this study, collected from the NW, NE and SE flanks of the Rwenzori (Fig. 1). Samples were collected from rift flanks to specifically target the locations of highest exhumation, while samples from the SE flank are part of the Mubuku River watershed and encompass ~2500 m elevation difference to constrain vertical motions (Fig. 1). All 12 samples produced AFT data, while 8 include counterpart AHe data (Table S1; TableS2).

3.2 Inverse thermal history modelling

Modelling of these data provides thermal histories of each rock sample that can be used to interpret exhumation, burial and rock uplift histories, alongside relevant geological information. Within this work, thermal modelling was completed using QTQt, a program that uses a Bayesian Transdimensional Markov Chain Monte Carlo algorithm to search time-temperature space and test numerous possible thermal histories against the input data (Gallagher, 2012). The resultant thermal history of a sample is an 'expected model' created from all possible histories and weighted by their posterior probability (Gallagher, 2012). This approach allows for the joint inversion of both AFT and AHe data as well as data from multiple samples. Fission-track data were modelled using the annealing model from Ketcham et al. (2007), using the diameter of the etched track pit parallel to c-axis (D_{par}) as an annealing parameter and c-axis corrected track lengths (Carlson et al., 1999; Donelick et al., 1999).

The intra-sample dispersion of single grain AHe ages is common for samples that have resided within the HePRZ for 10s of millions of years (Wildman et al., 2016). A broad range of AHe ages from a single sample, some older than counterpart AFT central ages, can make it difficult to effectively model thermal histories. If, however, this dispersion can be modeled, it can be exploited to provide effective thermal constraints. In an attempt to model dispersed ages, three additional steps were taken during thermal modelling: (i) the inclusion of a radiation damage model, (ii) the resampling of the additional activation energy required for helium trapped in damage vacancies (E_b) and (iii) the resampling of AHe error. The radiation damage model accounts for the change in helium diffusion kinetics due to development of damage vacancies in the crystal lattice caused by decay processes (e.g. alpha recoil, spontaneous fission and alpha emission). The model used is from Gerin et al. (2017) and describes how the energy required for He atoms to escape vacancies varies between individual grains and can be >50 kJ/mol (Gerin et al., 2017). Resampling of E_b between the values of 30 – 50 kJ/mol aims to improve AHe age predictions and produce more effective thermal history models. The resampling of AHe error during the inversion means single grain ages that consistently fail to fit with counterpart data can be effectively removed from the process by increasing their error.

3.3 χ-mapping and river profile modelling

Understanding the modern rock uplift history of the Rwenzori is achieved through analysing the modern drainage dynamics across the mountain range. We use two approaches, χ-mapping of the modern drainage systems and deriving uplift histories directly from river profiles. χ is a numerical proxy based on the geometry of a given fluvial system (Perron and Royden, 2012). This can be used to visualize areas within a drainage system undergoing changes in equilibrium, such as divide migration and river capture (Willett et al., 2014). The numerical value of χ for a specific point is the along channel integral of one over the upstream drainage area, scaled by a reference upstream drainage area raised to the power *m*, from the base level to this point and multiplied by a reference upstream drainage area (A_0 = 1 m^2). It can be thought of as a normalized landscape response time, such that information propagates from the base level to points of equal χ values. The comparison of χ values across drainage divides provides a useful interpretative tool for understanding drainage dynamics of a given system (Willett et al., 2014). Drainage divides with similar χ values on either side are interpreted as being in equilibrium, while divides with contrasting χ values are interpreted as being in disequilibrium, where the side with higher χ values is interpreted as the victim of drainage capture (Willett et al., 2014). A χ-map of the Rwenzori's was created using TopoToolbox (Schwanghart, & Scherler, 2014).

Estimating rock uplift histories from the river profiles across the Rwenzori is completed using the methodology outlined in Goren et al. (2014) and Fox et al. (2015). This approach converts the relationship between χ and elevation into a rock uplift rate through time and assumes; (i) rock uplift is spatially uniform across the catchment, (ii) bedrock erodibility is uniform in space and time and (iii) information propagates through the network independent of the local channel slope. Simply put, the elevation of a point on the river profile can be defined by the integral of normalized rock uplift rate between zero and the χ-value. Therefore, a linear model describing the χ and elevation relationship can provide an estimate of the normalized rock uplift rate (Goren et al., 2014). To account for noise in the data and to stabilize the model, a weighted least squares approach with a smoothing parameter is used (see Goren et al. (2014) and Fox et al. (2015) for details), that defines a total amount of rock uplift over an unknown, normalized time. Thermal history models provide estimates for the amount of uplift-induced exhumation over a known duration and therefore, an erodibility value (K) can be derived that provides an uplift rate that is consistent with the thermochronological data. Uplift models were completed on 7 rivers; 3 drainage systems that include samples and thermal histories from this study, 1 using a thermal history from a previous study (Mansour, 2016) and a further 3 using K values inferred from neighboring river systems.

4 Results

4.1 Apatite low-temperature thermochronology

AFT central ages range between 35.2 ± 2 Ma and 133.3 ± 8 Ma (Fig. 1), while c-axis corrected mean track lengths (MTLs) range between 13.21 ± 1.06 μm and 14.09 ± 1.13 μm (Table. S1). From the 12 AFT samples, 4 fail the chi-squared test (Galbraith, 2005), though only one sample (Rs47) is made of two age populations of which the older age population is defined by only a single anomalously old grain. D_{par} values, a kinetic parameter used to determine fission-track annealing behavior, range between 1.45 μm and 2.46 μm and broadly show positive correlations against AFT single grain ages, suggesting ages are dependent on variations in annealing characteristics (Carlson et al., 1999).

AHe single-grain ages range between 14 Ma - 321 Ma, with one anomalously old age (1429 Ma) that has been deemed as an outlier (Table. S2). Mean sample ages, calculated with this single removed age, range between 18 ± 4 Ma and 106 ± 66 Ma (Fig. 1) and display younger ages across the NW flank of the Rwenzori, while older ages are found on the eastern flank. Of the 8 samples, 3 show a positive trend against equivalent spherical radius (r'), while 6 show a positive trend against the effective uranium (eU) content, implying radiation damage and extended residence in the HePRZ may be a considerable factor in single grain age dispersion.

Comparisons between both the AFT and AHe data exhibit overlapping age ranges within 5 samples, highlighting the extent of dispersion with AHe samples, though mean AHe ages are lower than respective AFT ages in 6 samples, suggesting these overlapping age ranges may be driven by outliers. Additionally, the standard deviation of AHe samples, a proxy for dispersion, and mean AHe age against AFT age, both show a moderate positive correlation, implying samples with older AFT ages yield a greater amount of dispersion in AHe ages, likely due to extended residences in the HePRZ.

AFT and mean AHe ages against elevation show no obvious trend, suggesting that ages vary spatially across the study area. Notably, the highest sample (Rs30) produces a much younger Palaeocene age in comparison to surrounding samples, which show Cretaceous ages (Fig. 1). Age against distance to rift flank shows a trend of younger ages near the rift flanks, with the exception of samples from the NE flank (Rs47, Rs49 & Rs50) and sample Rs30, suggesting cooling and erosion of rift flanks may be a leading cause of age variation except in the NE of the region (Fig. 3).

Data from previous thermochronological studies from across the Rwenzori (Bauer et al., 2013; Mansour, 2016) (Fig. 2) allows for comparison of our new data to the wider dataset and review the spread of ages across the region. Longitudinal plots of AFT and AHe mean from the regional dataset clearly shows younger ages on the western side of the Rwenzori in comparison to older ages on the eastern side (Fig. 3).

4.2 Thermal history modelling

Results from thermal history modelling are shown for the NW and NE flank (Fig. 4) and the SE flank of the Rwenzori (Fig. 5). The NW flank of the Rwenzori incorporates three samples and two thermal histories from the rift flank. Rs44 exhibits linear protracted cooling throughout the Cenozoic at a rate of 1.3 °C/Myr (Fig. 4). A thermal history including both Rs71 and Rs72 exhibits four periods of cooling with an initial protracted cooling period until 30 Ma (1.5 °C/Myr), followed by accelerated cooling from 30 Ma to 20 Ma (3.4 °C/Myr), a period of slow protracted cooling between 20 Ma and 3 Ma (0.4 °C/Myr) and rapid cooling since 3 Ma (4 °C/Myr) (Fig. 4). The NE flank of the Rwenzori incorporates 3 samples, all taken from the rift flank. All three thermal histories outline linear protracted cooling histories throughout the Cenozoic with a cooling rate of 0.9 °C/Myr (Rs47), 0.73 °C/Myr (Rs49) and 0.4 °C/Myr (Rs50) (Fig. 4).

The SE flank encompasses 6 samples taken from elevations ranging between 3471 m and 1609 m. Sample Rs30 outlines a slow cooling rate (0.49 °C/Myr) until 5 Ma, followed by rapid cooling until present (7.4 °C/Myr) (Fig. 5). Rs31 shows a protracted Cenozoic cooling history at a rate of 0.57 °C/Myr to present (Fig. 5). Rs38 shows a three-stage history with a slow rate of cooling (0.32 °C/Myr) until 63 Ma, followed by a period of rapid cooling (2.7 °C/Myr) to 21 Ma and finishing with reheating (0.33 °C/Myr) to present (Fig. 5). Rs39 exhibits a linear protracted cooling throughout the Cenozoic at a rate of 1.01 °C/Myr until present (Fig. 5), while Rs40 displays cooling at a rate of 1.7 °C/Myr until 19 Ma when the rate lowers to 0.42 °C/Myr (Fig. 5). Finally, Rs43 displays a three-stage history with slow cooling (0.5 °C/Myr) until 55 Ma, followed by a period of accelerated cooling (1.3 °C/Myr) until 20 Ma and finishing with a period of reheating (0.25 °C/Myr) to present (Fig. 5).

Age and track length predictions from thermal histories vary with fission-track data being well predicted, while AHe data being poorly replicated. From the 12 samples analysed, the AFT central ages and mean track lengths were all replicated within error. In contrast, from the 40 AHe data only six ages were replicated within 10% error. From the remaining 34 ages, 30 were underpredicted (*predicted age* < *observed age*) implying that many of the analysed ages were older than expected, especially when compared to fission-track ages. There are many factors that can increase AHe ages (e.g. zoning, radiation damage, chemistry), particularly in samples with prolonged cooling through the PRZ, which cannot be accounted for in thermal modeling. Moreover, the bedrock sampled is either Proterozoic or Archaean in age implying that apatites may have experienced a complex thermal history that may have greatly affected the diffusion kinematics and inheritance of individual grains (Fox et al., 2019).

The thermal history modelling results presented here differ to the results of Bauer et al. (2013). Cenozoic cooling is confined to the Neogene in the results of Bauer et al. (2013) with any Paleogene cooling restricted to a much broader Late Cretaceous-Paleocene cooling event. These disparities may be due to differences in sampling strategy, prevalence of much older fission-track and (U-Th)/He ages, the use of recently developed helium diffusion models that account for radiation damage, and/or different modelling programs.

4.3 χ*-map*

χ-mapping of the Rwenzori exhibits a complex spread of χ values across the mountain range with higher values localised in the central region, around the highest topography, and in the northernmost boundary (Fig. 6). High χ values in the central region are predominantly on the eastern side of a major drainage divide separating eastern fluvial systems from western systems (a in Fig. 6). The westerly side of this divide exhibits lower χ values suggesting this divide is in disequilibrium and migrating eastwards, though this may also result from the effect of eastward regional tilting steepening and shortening rivers on the western side (Goren et al., 2014), implied from the regional geology and the thermochronology. High χ values in the north of the Rwenzori are found within a set of NE flowing fluvial systems on the northern side of a u-shaped drainage divide (b in Fig. 6). The southern side of this u-shaped divide exhibits much lower chi values from fluvial systems flowing either NW or SE, implying the drainage divide is in disequilibrium and is migrating northwards. The χ-map also highlights a major linear drainage divide that separates the NE flank from the NW flank and terminates in the central region (c in Fig. 6). The χ-values across the divide do not contrast significantly, though comparatively higher values are found in the NW side of the divide implying the divide is in disequilibrium and migrating NW. Though this could imply the NE flank is uplifting at greater rate, it is more likely a representation of the difference in base level on either side of the Northern Rwenzori (Fig. 1), creating lower χ values further upstream on the NE side.

An additional point of interest from χ-mapping is the nature of the headwaters of the river labeled 'River x' in Figure 6. The headwaters of this river appear to initially flow east before abruptly redirecting north, suggesting river capture has occurred. The easterly direction of the headwaters suggests it may have previously connected to the river east of the drainage divide, labeled 'River y' in Figure 6, and uplift of the landscape has caused the headwaters to be captured by River x. This would imply recent tectonism in the Central Rwenzori and may explain why drainage divides a and c are not connected (Fig. 6), as would be expected of a simple horst structure.

4.4 River profile modelling

Uplift models were extracted from 7 river catchments. 4 models use an erodibility value (K) constrained from thermal models present in each catchment (Fig. 7; a, b, c, d) (Supplementary Data), and an additional 3 from neighboring catchments (Fig. 7; a-i, b-i, d-i), in which K is inferred from the neighbouring rivers, assuming it does not significantly change over this relatively short distance (Fig. 7). Calibration of these models requires rock uplift rate histories to be converted to cumulative rock uplift histories and then compared to the exhumation histories (Figure S1). As thermochronological samples are close to baselevel, the rock uplift rates here are likely equal to the exhumation rate.

Results from river profile modelling show a clear dichotomy between the south-eastern flank and western flank of the Rwenzori. Along the SE flank, river *a* records uplift from 40 Ma, showing a rise in uplift rate from 20 m/Myr to 63 m/Myr between 35 Ma and 18 Ma, before declining to 16 m/Myr at present (Fig. 7). This is mimicked by the uplift history of river *a-i*, which records uplift from 37 Ma onwards showing a gradual increase in uplift rate from 30 m/Myr to 66 m/Myr between 37 Ma and 18 Ma, before a decline to 20 m/Myr at present (Fig. 7).

Along the NW flank of the Rwenzori, river *b* resolves an uplift history of only 16 Ma. This is because of the shorter rivers, and thus smaller χ-values, found across this area. The history exhibits a decline in uplift rate from 70 m/Myr to 50 m/Myr between 15 Ma and 9 Ma, followed by an increase to 65 m/Myr at present (Fig. 7). This is similar to the history recorded in river *c*, which also resolves a history from 15 Ma to present, showing a small decline from 55 m/Myr to 53 m/Myr between 15 Ma and 10 Ma and a gradual increase back to 55 m/Myr at present day (Fig. 7). This uplift history is the same in river *b-i* that records an uplift history from 20 Ma onwards, exhibiting a decline from 75 m/Myr to 52 m/Myr between 20 Ma and 10 Ma, followed by a gradual rise to 64 m/Myr at present day (Fig. 7).

Along the western flank of the Rwenzori, river *d* resolves an uplift history from 16 Ma to present, exhibiting a sharp decline in uplift rate from 151 m/Myr to 111 m/Myr between 16 Ma and 11 Ma, followed by two small pulses of increased uplift, reaching 121 m/Myr, at 9 Ma and 6 Ma followed by a sharp increase to 134 m/Myr at present (Fig. 7). River *d-i* resolves an uplift history from 18 Ma to present and initially outlines a decline in uplift rate from 123 m/Myr to 86 m/Myr between 18 Ma and 13 Ma followed by an increase back to 123 m/Myr at present day (Fig. 7).

These models provide insight into the uplift history of the Rwenzori; however, it is important to recognize the limitations in the approach. Firstly, these models assume rock uplift rate is spatially uniform across the river catchment, which may be unlikely as we see different thermal histories at the outlets of the catchments suggesting regional tilting. Eastward tilting can lead to differences in the χ-elevation relationship that would lead to apparent accelerating uplift (i.e., steepening rivers) on the western side and decelerating uplift (i.e., shallowing rivers) on the eastern side. The presence of the low rates of rock uplift resolved during the earliest time intervals across the eastern catchments suggest that this tilting is not the dominant signal and that the rivers are responding to transient signals and therefore the assumption of spatially uniform rock uplift is suitable. Secondly, this approach assumes that the topography is formed by fluvial erosional processes in response to rock uplift. There is clear evidence for glacial erosion at high elevations and this may also lead to anomalous rock uplift rates; however, the equilibrium-line altitude in the region is ~4500 m and makes up <0.5% of the landscape implying the influence of glaciers is negligible. Thirdly, due to the Rwenzori's relatively limited size (~3000 km^2), many of the river systems are short and can only resolve a certain amount of information on a small timescale (<40 Myr). This is highlighted by comparing rivers *a* and *b,* which contrast greatly in length (37.1 km and 1.4 km, respectively) and temporal resolution (40 Myr and 15 Myr, respectively) showing longer rivers provide longer temporal resolution. Finally, it is important to note that the uncertainties on the inferred uplift rate histories can be quite large. These uncertainties relate to the choice of the damping parameter and the erodibility value for each river basin (Figure S1 and S2), however, the overall trends and magnitude of cumulative rock uplift are robust.

5 Discussion

5.1 Uplift history of the Rwenzori Mountains

Spatial disparity between thermochronometric ages, thermal histories and uplift histories across the flanks of the Rwenzori suggests each flank experienced differing rock uplift and exhumational histories throughout the Cenozoic. The SE flank of the Rwenzori appears to have experienced significant uplift between the Eocene and early Miocene, with later uplift occurring away from the rift margin in the late Miocene–Pliocene. Thermal histories outline either protracted cooling throughout the Cenozoic, periods of accelerated cooling throughout the Eocene and Oligocene or rapid cooling in the late Miocene–Pliocene (Fig. 5). Differences in fission track ages and thermal history results between Rs38, Rs39 and Rs40 may result from a fault between samples, as previously noted in Bauer et al. (2010), however, until detailed mapping of the area is completed this is difficult to identify effectively. These results imply the SE flank experienced exhumation and uplift during the Paleogene, with the latter stage of cooling likely resulting from localised uplift away from the rift flank. This is supported by uplift histories derived from river profiles that resolve a significant uplift phase between 35 Ma and 18 Ma reaching a maximum of 63 m/Myr (Fig. 7). The short length of these river profiles means the uplift history >40 Ma cannot be resolved; however, thermal history models imply earlier uplift phases may have occurred in the Eocene (Fig. 5; Rs38, Rs40 & Rs43).

The NE flank of the Rwenzori appears to have experienced only limited uplift during the Cenozoic expressed by old thermochronometric ages (Figs. 2 and 3) and protracted cooling in thermal histories. This suggests rock uplift magnitude has been <2 km and has failed to expose young thermochronometric ages (Fig. 4). This is consistent with the geomorphology of the NE flank, where the landscape to the east is an elevated plateau >900 m higher than the landscapes surrounding all other flanks of the Rwenzori (Fig. 1). It has been postulated this elevated plain is the result of the Lake George Rift's failure to propagate northward (Koehn et al., 2016), causing only minor uplift along the NE flank.

The NW flank of the Rwenzori formed through two uplift phases occurring in the Oligocene and the late Miocene–Pliocene. Fission-track and (U-Th)/He ages range from the Eocene to Miocene (Fig. 1) and thermal history models outline either protracted cooling or a four-phase cooling history with accelerated cooling in the Oligocene and late Miocene–Pliocene (Fig. 4). This suggests the rate of exhumation increased during these times, likely due to fault-driven uplift of the flank, though it should be noted the most recent cooling event occurs outside the HePRZ and may be a modelling artefact. This is supported by river profile models which exhibit a rise in rock uplift rate in the Miocene (11 Ma) and fail to resolve an Oligocene event due to the limited length of the studied rivers (<3 km) (Fig. 7), though the decrease in uplift rate from 16 Ma to 9 Ma implies rates may have been higher prior to 16 Ma. Importantly, the uplift rates taken from the NW flank appear to increase from north to south, a trait that is consistent with the rise in topography toward the south and highlights the variability of uplift rates across the Rwenzori.

The western flank of the Rwenzori shows uplift histories from river profiles, constrained from thermal histories from Mansour (2016), exhibiting very high uplift rates (~120 m/Myr), following an increase in rate during the Miocene (Fig. 7). These results are consistent with the southward trend of increasing uplift rates along the NW and W flank, explaining the western flanks elevated topography (Fig. 7). Moreover, though both rivers *d* and *d-i* are too short to resolve an uplift history before 20 Ma, they do show a significant decrease in rock uplift rate between 18 Ma and 11 Ma, suggesting elevated rates of rock uplift may have occurred prior to 20 Ma (Fig. 7). This is consistent with the rock uplift history derived from the NW and SE flanks and further implies the whole region was uplifting in the Palaeogene, while only the western side saw renewed rock uplift in the late Miocene–Pliocene (Fig. 8). Moreover, rock uplift on the western side of the Rwenzori accounts for the chi values along the central drainage divide in the chi-map, where lower values to the west imply the drainage divide is migrating east, likely driven by greater rock uplift on the western side (Fig. 6).

This interpretation of the Rwenzori uplift history fails to correlate with the interpreted history from stratigraphic studies (Pickford et al., 1992; Schneider et al., 2016). Miocene strata to the NE of the Rwenzori show a petrological change in sediment around ~5.5 Ma, implying surface uplift of the Rwenzori began at this time (Schneider et al., 2016). Moreover, biostratigraphic work of the surrounding lakes suggests they were all linked as the paleo-lake Obweruka, which was separated by the rising Rwenzori in the late Miocene (Pickford et al., 1992). The rock uplift history presented here, alongside the perceived age of paleo-lake Obweruka, suggests it is more likely the Rwenzori acted as an elevated peninsula within the Lake Obweruka throughout much of the Miocene, with only the late Miocene uplift event effectively resolved in the documented stratigraphy. As such, it is unlikely the paleo-lake Obweruka fully covered the mountain range, implied by the absence of Cenozoic sedimentary rocks within the Rwenzori that would likely have been preserved due to the documented low rates of erosion (Roller et al., 2012).

5.2 Mechanism of rock uplift

Our interpretation of the Rwenzori's spatially differential rock uplift histories infers two main phases of rock uplift have occurred during the Cenozoic: Eocene-Oligocene and late Miocene-Pliocene (Fig. 9). These findings require rock uplift mechanisms that account for the rapid rock uplift on short timescales (<2.3 Ma) are now unnecessary (Ring, 2008; Wallner & Schmeling, 2010) and processes that incorporate a longer uplift history must be recognized. Previous studies on the fault kinematics of the Rwenzori concluded the mountain range is rotating clockwise due to the interaction of both the Lake Albert and Lake George rifts (Koehn et al., 2008; Sachau et al., 2013). Numerical modelling of this rift interaction, encompassing a stiff elastic horst block between the two, highlights the creation of a unique stress field that bends the brittle lithosphere of the central horst block upwards and drives significant rates of rock uplift while also allowing the underlying Moho to rise (Sachau et al., 2013). This mechanism predicts the rock uplift of the Rwenzori effectively and is also consistent with estimates of Moho depth across the region that show a significant rise under the central Rwenzori (~22 km) compared to the surrounding lithosphere (~30 km) (Gummert et al., 2016).

Importantly, similar numerical models that incorporate relevant faults within the Rwenzori, show brittle deformation transfers away from the rift margin, effectively shifting the location of maximum uplift into the center of the Rwenzori (Fig. 9c), an event highlighted in our interpretation of the SE flank. The transfer of uplift away from the rift flank in late Miocene–Pliocene is supported by the thermal history of sample Rs30, geomorphology and χ values from the central Rwenzori. The thermal history model of Rs30 outlines the onset of rapid cooling at ~5 Ma (7.4 °C/Myr) to present (Fig. 9a), implying exhumation of the surface suddenly intensified, likely due to tectonic activity. The geomorphology of the sample site appears to verify this, characterised by a steep sided valley (topography envelope 700 – 1000 m) that abruptly ends at the inferred northern extent of the Ibimbo Fault (Fig. 9b). Moreover, should the Ibimbo Fault continue further north, it would also explain the proposed river capture between rivers x and y, as shown in the chi-map (Fig. 6; Fig. 9). Uplift of the inferred Ibimbo Fault's footwall in the late Miocene–Pliocene would have likely caused a redirection in flow pathways instigating the capture of river x's headwaters from river y (Fig. 6; Fig. 9). The absence of an increase in uplift rate on the SE rift margin suggests brittle deformation and uplift transferred westward to the Ibimbo Fault in the late Miocene (Fig. 9).

The transfer of deformation and uplift from the SE rift margin westward to the inferred Ibimbo Fault (Fig. 9) can be explained through the stalling of the Lake George Rift in the late Miocene. This lack of rifting may be due to the NW-SE fabric within the Buganda-Toro metamorphic belt, stopping further propagation of the rift northwards and effectively stalling it (Koehn et al., 2016). Numerical modelling of stalled rifts highlights how the termination of rift propagation will lead to horizontal stress and deformation being distributed widely across the area near the tip rift propagation (Van Wijk & Blackman, 2005). In the case of the Rwenzori, this redistribution of stress may have caused uplift to transfer from the rift margin to the Ibimbo Fault in the late Miocene, creating the modern geomorphology of the Rwenzori.

5.3 Implications for the history of the East African Rift

The results presented here suggest the Rwenzori's began uplifting in the Eocene, incorporating two phases of uplift in the Eocene–Oligocene and late Miocene–Pliocene (Fig. 8). This interpretation is contentious as active rifting across the Western Branch of the EARS is believed to have initiated in the Miocene (Ebinger, 1989; Morley & Ngenoh, 1999) and thus much later than in the Eastern Branch where rifting began in the Eocene (Morley & Bosworth, 1999). Though the Miocene age for the Western Branch initiation is the widely held hypothesis, magnetostratigraphy, tephrostratigraphy and the detrital geochronology of sediment from the Rukwa Rift Basin, in the southern Western Branch, suggests active rifting began in the Oligocene (Roberts et al., 2012). This corresponds to previous thermochronological studies from the Western Branch that outline the onset of cooling in thermal models in the Eocene (50 Ma – 40 Ma) (van der Beek et al., 1998; Bauer et al., 2010), implying uplift of the landscape may have started even earlier. Moreover, uplift in the Eocene correlates with other geological phenomena in the region, such as the redirection of the Nile (Underwood et al., 2013) and the Congo rivers (Stankiewicz & de Wit, 2006), and is consistent with the timing of rift initiation from thermochronological work in the Eastern Branch (Boone et al., 2019). Boone et al. (2019) presents thermal history models from the rift flanks of the Turkana Depression that highlight accelerated cooling from the Eocene to Miocene, initiating at 45 Ma, while similar studies across the Eastern Branch have also highlighted cooling episodes in the Late Cretaceous–Paleocene and late Miocene–Pliocene (Foster & Gleadow, 1996; Spiegel et al., 2007). Our results effectively unite the two branches of the EARS temporally and provides the means for generating a universal mechanism for the formation of the entire rift system.

The underlying mechanism that formed the EARS remains a highly debated topic, with both 'active' and 'passive' mechanisms postulated (Chorowicz, 2005). Though this study does not offer greater insight into a wider mechanism, it supports the notion of contemporaneous rifting across the EARS in the Paleogene which correlates to numerous tectonic processes including rifting phases in Northern Kenya and Sudan (Bosworth, 1992; Morley, 1992), kinematic changes across the Indian Ocean (Cande et al., 2010) and the broader collision of African into Eurasia (Rosenbaum et al., 2002). This may suggest extension across the EARS was driven by large-scale passive tectonic processes, though active plume-related processes that initiate contemporaneous rifting must also be recognized (Koptev et al., 2015). Further studies of sediments within rift basins across the region, such as Lake Albert, Lake Rukwa and Lake Tanganyika, are necessary to effectively determine the timing of extensional onset. Although attempts are being made to investigate deeper sequences in rift lakes (Russell et al., 2012), stratigraphic evidence to support early initiation of rifting remains elusive. The results of this work alongside previous studies suggest the topography of the Western Brach of the East African Rift likely dates back to the Eocene and thus, the modern consensus on rift initiation requires review.

6 Conclusions

Apatite fission-track and (U-Th)/He analysis, coupled with thermal history and river profile modelling suggest the Rwenzori Mountains formed through multiple phases of uplift beginning in the Eocene. We suggest the Rwenzori have experienced spatially varying uplift and exhumation histories throughout the Cenozoic, with the western flank experiencing much greater amounts of uplift compared to the eastern flank. This is supported by spatial trends in thermochronological data and thermal history modeling, which display higher rates of cooling across the NW flank and much slower rates of cooling across both the NE and SE flanks. Uplift histories derived from river profiles reveal a significant phase of uplift in the Eocene–Oligocene and another in the late Miocene–Pliocene, that is continuing at present along the western flank. This dichotomy in uplift histories across the region suggest uplift was instigated due to the interaction of two propagation rift centers, the Lake Albert and Lake George rifts, leading to rapid uplift of the central horst block, likely caused by the stiffness of the brittle crust and asthenospheric upwelling. As no late Miocene–Pliocene uplift is recorded on the eastern flank it is likely the Lake George Rift stopped propagating in the late Miocene, due to a contrasting fabric in the underlying basement, and uplift migrated west to the Ibimbo Fault at the center of the Rwenzori. These results have broad implications for the rifting history of the Western Branch of the EAR, implying rift initiation began in the

Eocene–Oligocene, parallel with rift initiation in the Eastern Branch of the EAR and consistent with a growing catalogue of research and regional geological phenomena.

Acknowledgements

We thank the Ugandan National Council for Science and Technology (UNCST) and Uganda Wildlife Authority (UWA) for the permission to undertake research in Uganda (project NS582, Understanding the structure, permeability and activity of faults in and around the Rwenzori mountains, Albertine rift system, Uganda). We also thank Dr. Andreas Schumann for his help in the field. SJ's postdoctoral fellowship at the University of Calgary is funded by the University of Calgary and EE's NSERC Discovery Grant (RGPIN-2018-03932). MF is supported by NERC (NE/N015479/1). Financial support for fission-track analysis was provided by the University of Calgary, while (U-Th)/He analysis was supported by the Daniel Pidgeon fund from The Geological Society.

Figures

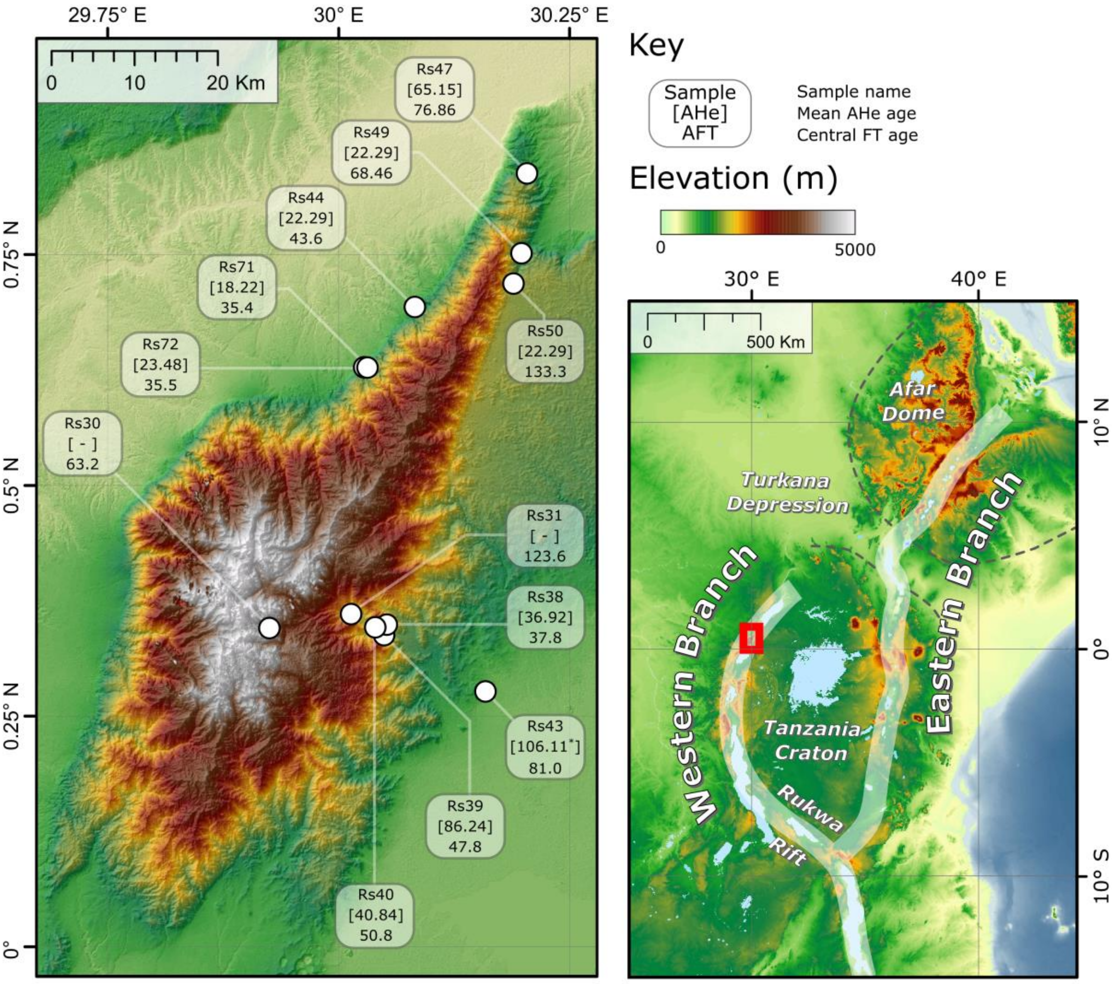

(Figure. 1) Digital elevation model of the Rwenzori and the East African Rift System. Sample locations highlighted with sample name, mean AHe age (square brackets) and AFT central ages shown. The asterisk on the mean AHe age from sample Rs43 highlights that this value has been calculated following the removal of one anomalously old AHe age (>1 Ga) (Table. S2). The wider map of the East African Rift highlights the Rwenzori's location in the Western Branch (red box) and the location of important features in the region.

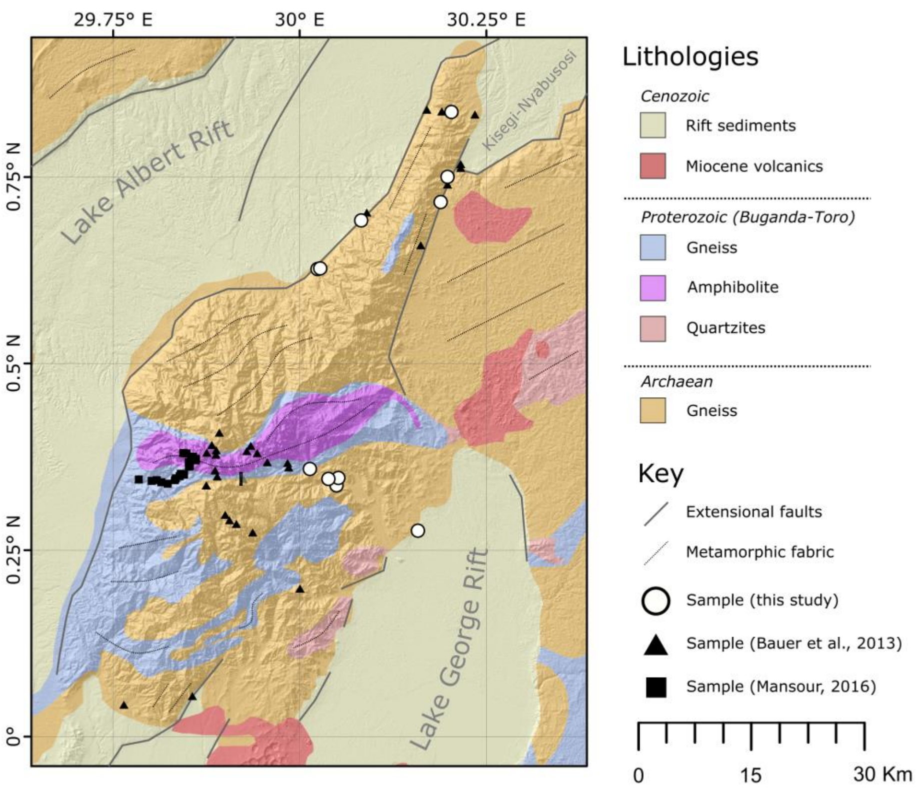

(Figure. 2) Simplified geological map of the Rwenzori Mountains, Uganda, with sample locations from this study and previous studies marked; adapted from Koehn et al. (2016) and Schneider et al. (2016). The basement of the Rwenzori is principally made up of Archaean gneisses and Proterozoic amphibolite and metasediments. Cenozoic volcanics and sediments are found on the flanks, formed/deposited during extension of the Lake Albert and Lake George rifts.

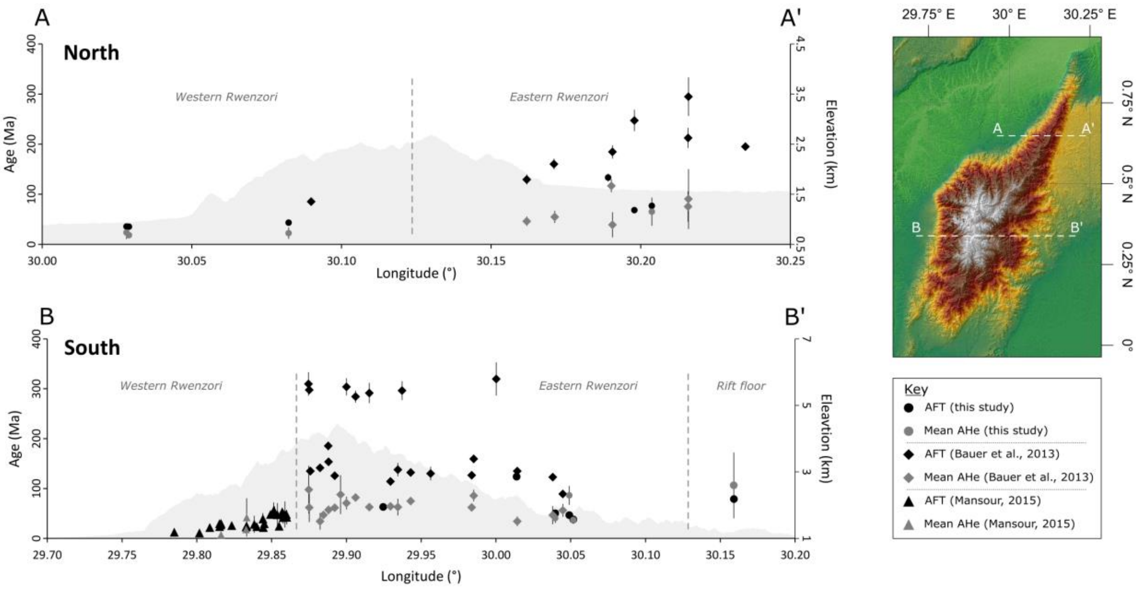

(Figure. 3) Cross sections across the northern (A–A') and southern (B–B') regions of the Rwenzori displaying apatite fission track (AFT) central ages and mean apatite (U-Th)/He (AHe) ages from this study and two previous studies (Bauer et al., 2013; Mansour, 2016). Spatial trends show the western side of the Rwenzori consistently has lower AFT central ages and mean AHe age when compared to the eastern side, suggesting great amount of cooling has occurred on the western side, possibly through enhanced exhumation and rock uplift.

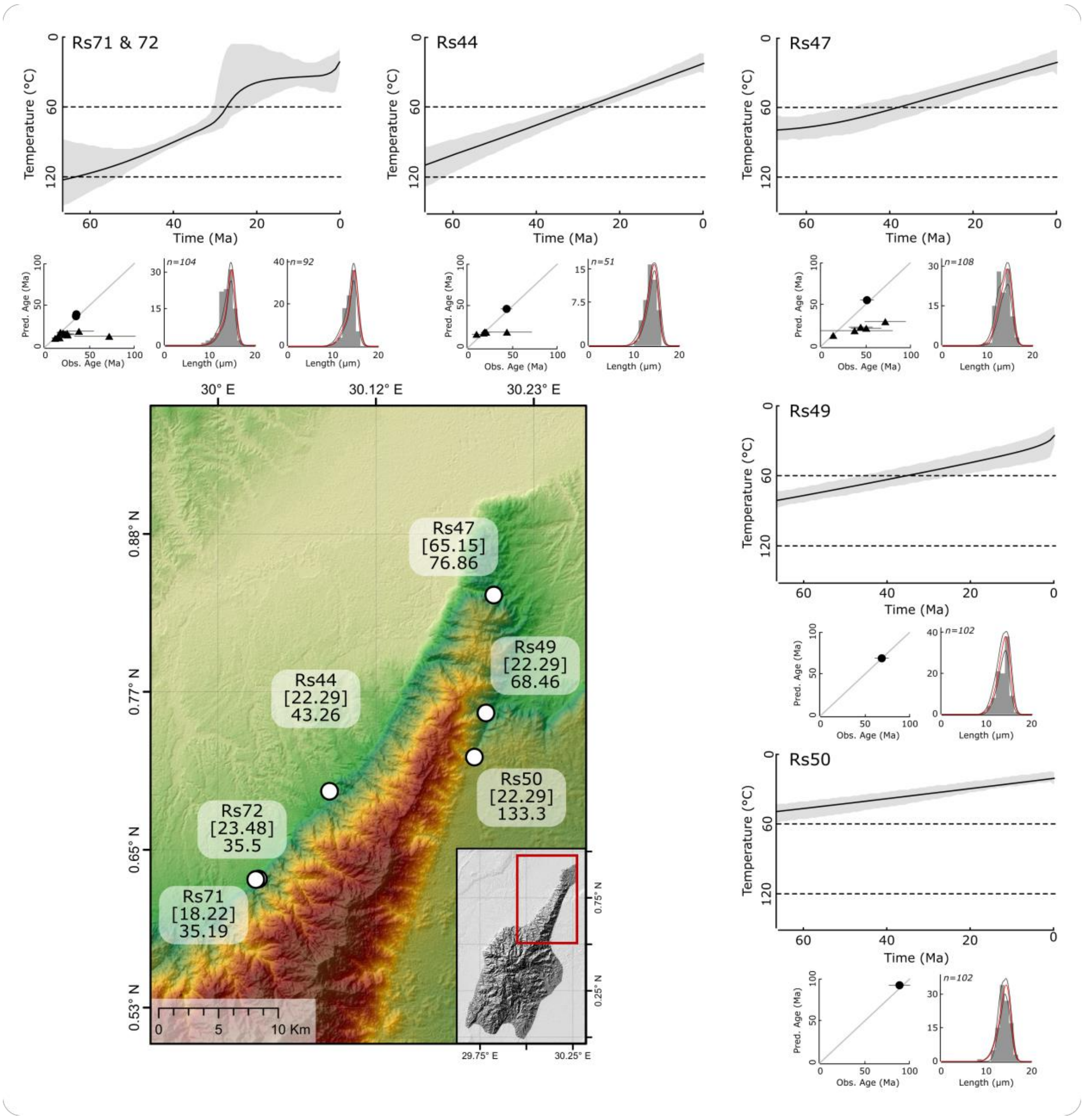

(Figure. 4) Thermal history models from the northern portion of the Rwenzori with age and track length distribution predictions. The black line within each thermal history is the 'expected model' and the grey shaded area outlines the 95% credible intervals. Age predictions are shown in the observed age against predicted age plots, where ● = AFT central ages and ▲ = single grain AHe ages. Measured track length distribution (c-axis corrected) are shown in grey histograms, while the predicted distribution with 95% credible intervals are displayed in red and grey respectively. Results show that greater cooling has occurred on NW flank compared to the NE flank and two phases of accelerated cooling occurred in the Oligocene-Miocene and late Miocene-Pliocene (Rs71 & 72).

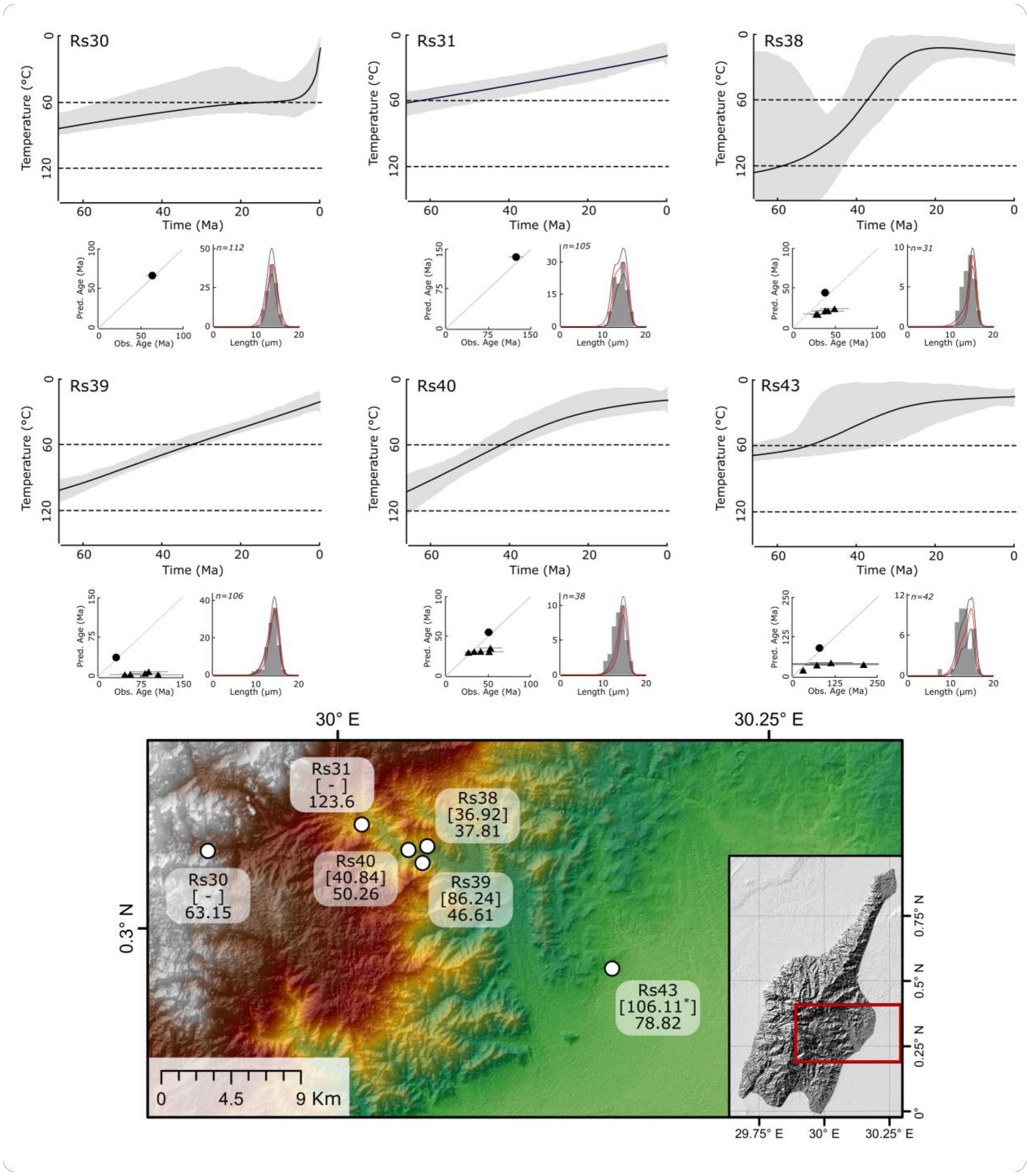

(Figure. 5) Thermal history models from the southern portion of the Rwenzori with age and track length distribution prediction outlined below. The black line within each thermal history is the 'expected model' and the grey shaded area outlines the 95% credible intervals. Age predictions are shown in the observed age against predicted age plots, where ● = AFT central ages and ▲ = single grain AHe ages. Measured track length distribution (c-axis corrected) are shown in grey histograms, while the predicted distribution with 95% credible intervals are displayed in red and grey respectively. Results show either protracted cooling of accelerated cooling throughout the Paleogene, while localised rapid cooling has occurred at the highest elevations (Rs30).

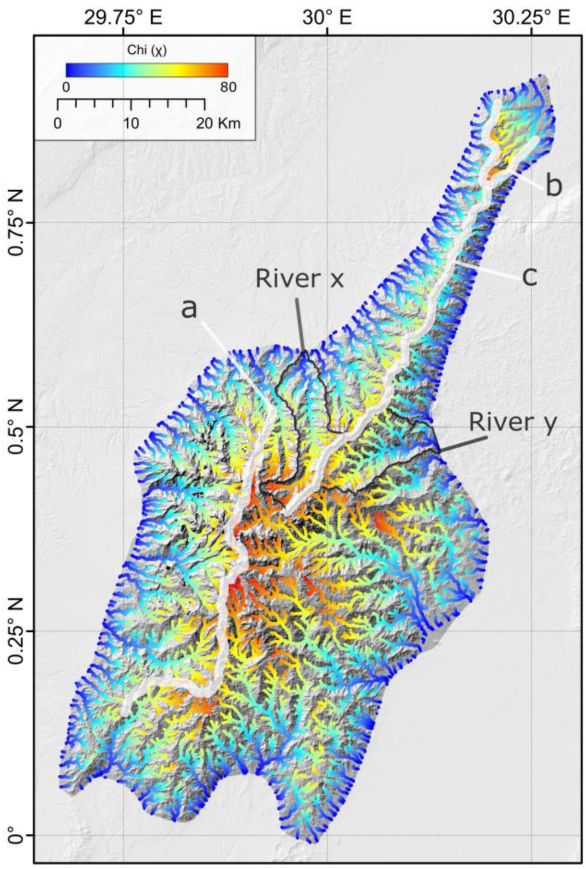

(Figure. 6) Chi-map of the Rwenzori Mountains created using TopoToolbox (Schwanghart, & Scherler, 2014). Results highlight three major drainage divides (a, b & c) and the catchments of rivers x and y. Chi values in the south imply uplift is likely higher on the western side, while in the north uplift is higher on the eastern side, though the latter is likely due to differing base levels. The headwater of River x suggests it was initially part of River y and were captured likely due to tectonic forcing in the late Miocene. This would also explain why drainage divides a and b are not connected, as would be expected in a typical horst structure.

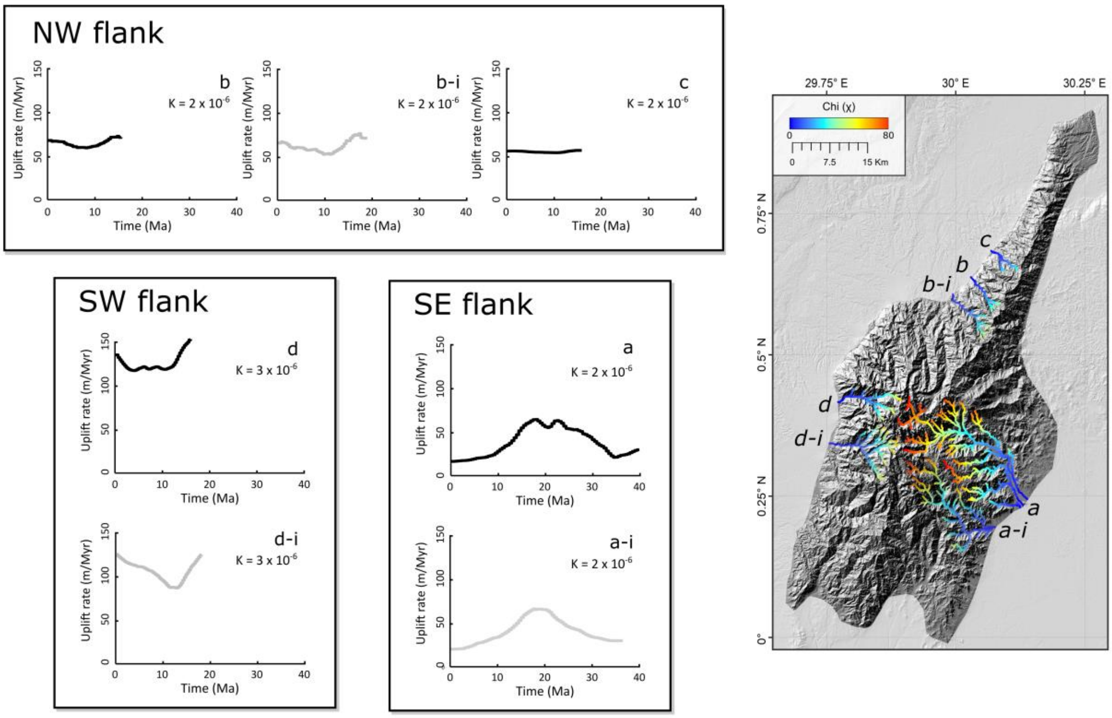

(Figure. 7) Results from river profile modelling outlining uplift histories from the SW, NW and SE flanks of the Rwenzori. Results shows that uplift histories differ on either side of the Rwenzori with the eastern flank experiencing the majority of uplift in the Oligocene-Miocene and the western flank in the late Miocene-Pliocene.

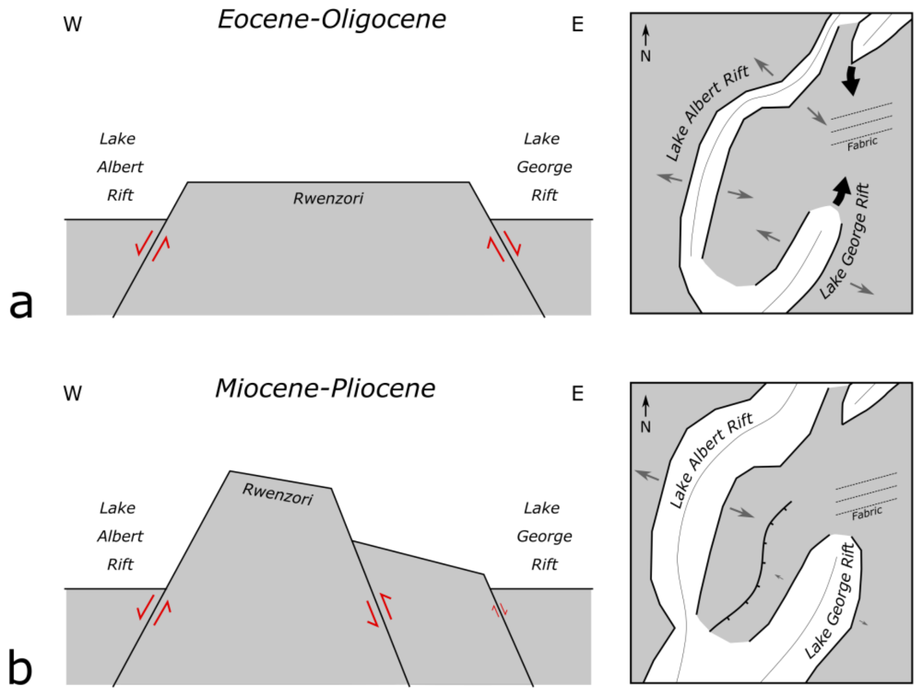

(Figure. 8) Summary of the proposed uplift history of the Rwenzori. Schematic cross section and tectonic map during the (a) Eocene–Oligocene onset of rifting, and (b) late Miocene–Pliocene reactivation.

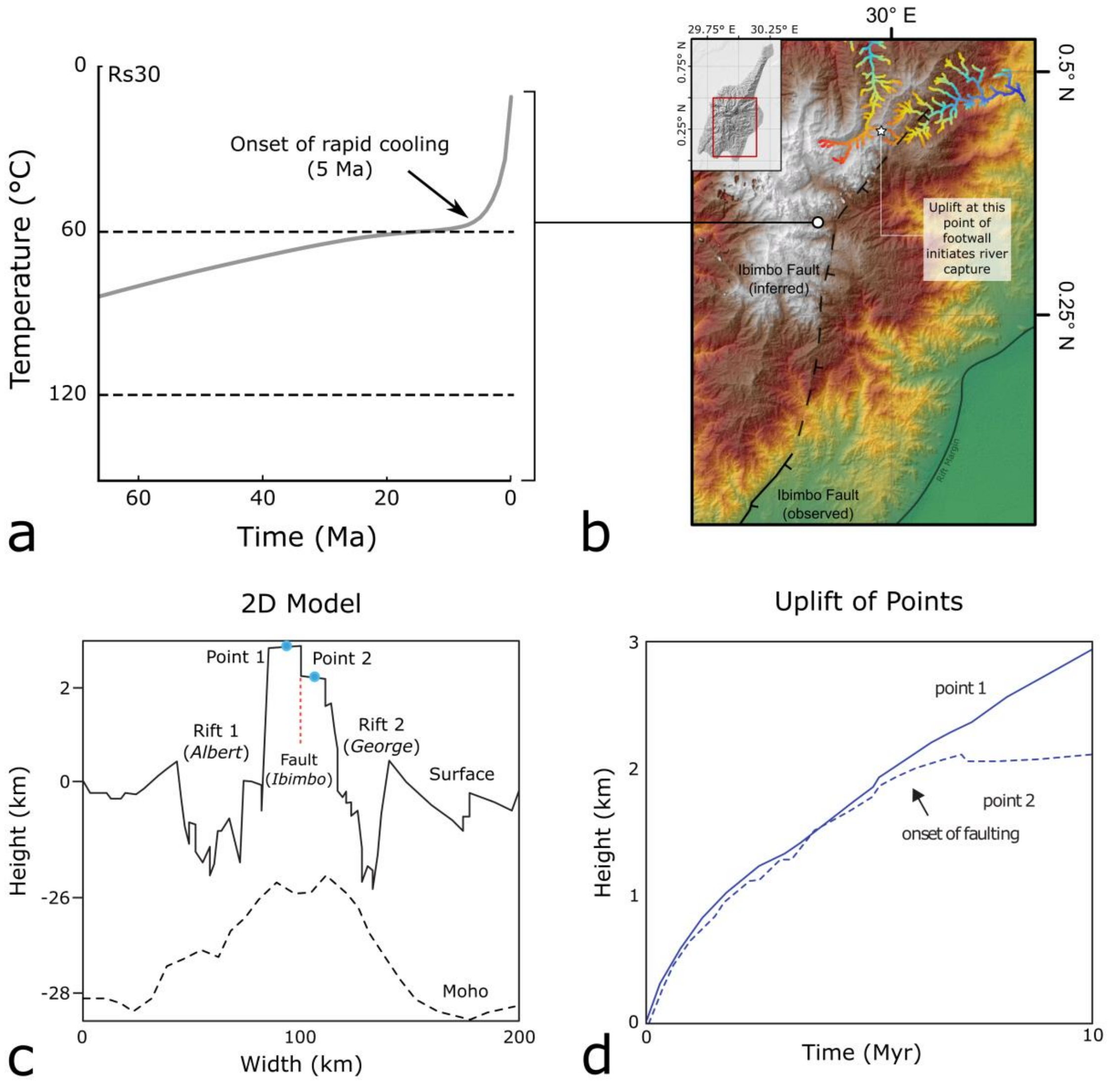

(Figure. 9) Results from this work and Sachau et al. (2013) outlining the uplift of the inferred Ibimbo Fault in the late Miocene–Pliocene. (a) Thermal history from sample Rs30 (b) Map of southern Rwenzori that displays the observed extent of the Ibimbo Fault and the inferred extent derived from geomorphology and the possible river capture of river x's headwaters. (c) Results of numerical modeling from Sachau et al. (2013) that incorporates a major central fault in the center of a rigid horst block. Rifting on either side of the horst block leads to a dramatic rise of the horst's topography and the underlying Moho, though uplift of the western side of the block appears greater than the eastern due to the central fault. (d) Cumulative uplift histories of Point 1 and Point 2 in (c) outlining that both uplift at the same rate until ~6 Ma, where the central fault causes Point 1 to keep uplifting and Point 2 to cease uplifting.

References

Bauer, F.U., Glasmacher, U.A., Ring, U., Karl, M., Schumann, A. and Nagudi, B., 2013. Tracing the exhumation history of the Rwenzori Mountains, Albertine Rift, Uganda, using low-temperature thermochronology. Tectonophysics, 599, pp.8-28.

Bauer, F.U., Glasmacher, U.A., Ring, U., Schumann, A. and Nagudi, B., 2010. Thermal and exhumation history of the central Rwenzori Mountains, Western rift of the east African rift system, Uganda. International Journal of Earth Sciences, 99(7), pp.1575-1597.

Bauer, F.U., Karl, M., Glasmacher, U.A., Nagudi, B., Schumann, A. and Mroszewski, L., 2012. The Rwenzori Mountains of western Uganda–Aspects on the evolution of their remarkable morphology within the Albertine Rift. Journal of African Earth Sciences, 73, pp.44-56.

Boone, S.C., Kohn, B.P., Gleadow, A.J., Morley, C.K., Seiler, C. and Foster, D.A., 2019. Birth of the East African Rift System: Nucleation of magmatism and strain in the Turkana Depression. Geology, 47(9), pp.886-890.

Bosworth, W., 1985. Geometry of propagating continental rifts. Nature, 316(6029), pp.625-627.

Bosworth, W., 1992. Mesozoic and early Tertiary rift tectonics in East Africa. Tectonophysics, 209(1-4), pp.115-137.

Cande, S.C., Patriat, P. and Dyment, J., 2010. Motion between the Indian, Antarctic and African plates in the early Cenozoic. Geophysical Journal International, 183(1), pp.127-149.

Carlson, W.D., Donelick, R.A. and Ketcham, R.A., 1999. Variability of apatite fission-track annealing kinetics: I. Experimental results. American mineralogist, 84(9), pp.1213-1223.

Chorowicz, J., 2005. The east African rift system. Journal of African Earth Sciences, 43(1-3), pp.379-410.

Donelick, R.A., Ketcham, R.A. and Carlson, W.D., 1999. Variability of apatite fission-track annealing kinetics: II. Crystallographic orientation effects. American Mineralogist, 84(9), pp.1224-1234.

Ebinger, C.J., 1989. Tectonic development of the western branch of the East African rift system. Geological Society of America Bulletin, 101(7), pp.885-903.

Fox, M., Bodin, T. and Shuster, D.L., 2015. Abrupt changes in the rate of Andean Plateau uplift from reversible jump Markov Chain Monte Carlo inversion of river profiles. Geomorphology, 238, pp.1-14.

Fox, M., Dai, J.G. and Carter, A., 2019. Badly behaved detrital (U-Th)/He ages: Problems with He diffusion models or geological models?. Geochemistry, Geophysics, Geosystems, 20(5), pp.2418-2432.

Galbraith, R.F., 2005. Statistics for fission track analysis. CRC Press.

Gallagher, K., 2012. Transdimensional inverse thermal history modeling for quantitative thermochronology. Journal of Geophysical Research: Solid Earth, 117(B2).

Gallagher, K., Brown, R. and Johnson, C., 1998. Fission track analysis and its applications to geological problems. Annual Review of Earth and Planetary Sciences, 26(1), pp.519-572.

Gautheron, C., Tassan-Got, L., Ketcham, R.A. and Dobson, K.J., 2012. Accounting for long alpha-particle stopping distances in (U–Th–Sm)/He geochronology: 3D modeling of diffusion, zoning, implantation, and abrasion. Geochimica et Cosmochimica Acta, 96, pp.44-56.

Gerin, C., Gautheron, C., Oliviero, E., Bachelet, C., Djimbi, D.M., Seydoux-Guillaume, A.M., Tassan-Got, L., Sarda, P., Roques, J. and Garrido, F., 2017. Influence of vacancy damage on He diffusion in apatite, investigated at atomic to mineralogical scales. Geochimica et Cosmochimica Acta, 197, pp.87-103.

Goren, L., Fox, M. and Willett, S.D., 2014. Tectonics from fluvial topography using formal linear inversion: Theory and applications to the Inyo Mountains, California. Journal of Geophysical Research: Earth Surface, 119(8), pp.1651-1681.

Gummert, M., Lindenfeld, M., Wölbern, I., Rümpker, G., Celestin, K. and Batte, A., 2016. Crustal structure and high-resolution Moho topography across the Rwenzori region (Albertine rift) from P-receiver functions. Geological Society, London, Special Publications, 420(1), pp.69-82.

Ketcham, R.A., Carter, A., Donelick, R.A., Barbarand, J. and Hurford, A.J., 2007. Improved modeling of fission-track annealing in apatite. American Mineralogist, 92(5-6), pp.799-810.

Koehn, D., Aanyu, K., Haines, S. and Sachau, T., 2008. Rift nucleation, rift propagation and the creation of basement micro-plates within active rifts. Tectonophysics, 458(1-4), pp.105-116.

Koehn, D., Link, K., Sachau, T., Passchier, C.W., Aanyu, K., Spikings, A. and Harbinson, R., 2016. The Rwenzori Mountains, a Palaeoproterozoic crustal shear belt crossing the Albertine rift system. International Journal of Earth Sciences, 105(6), pp.1693-1705.

Koptev, A., Calais, E., Burov, E., Leroy, S. and Gerya, T., 2015. Dual continental rift systems generated by plume–lithosphere interaction. Nature Geoscience, 8(5), pp.388-392.

Link, K., Koehn, D., Barth, M.G., Tiberindwa, J.V., Barifaijo, E., Aanyu, K. and Foley, S.F., 2010. Continuous cratonic crust between the Congo and Tanzania blocks in western Uganda. International Journal of Earth Sciences, 99(7), pp.1559-1573.

MacPhee, D., 2006. Exhumation, rift-flank uplift, and the thermal evolution of the Rwenzori Mountains determined by combined (U-Th)/He and U-Pb thermochronometry (Doctoral dissertation, Massachusetts Institute of Technology).

Mansour, S.E.E., 2016. Long-term topographic evolution of the African plate, causes and consequences for surrounding lithospheric plates (Doctoral dissertation).

McDougall, I.. and Brown, F.H., 2009. Timing of volcanism and evolution of the northern Kenya Rift. Geological Magazine, 146(1), pp.34-47.

Misra, A.A. and Mukherjee, S., 2015. Tectonic inheritance in continental rifts and passive margins. Springer International Publishing.

Morley, C.K. and Ngenoh, D.K., 1999. AAPG Studies in Geology# 44, Chapter 1: Introduction to the East African Rift System.

Morley, C.K., Cunningham, S.M., Harper, R.M. and Wescott, W.A., 1992. Geology and geophysics of the Rukwa rift, East Africa. Tectonics, 11(1), pp.69-81.

Mortimer, E., Kirstein, L.A., Stuart, F.M. and Strecker, M.R., 2016. Spatio-temporal trends in normal-fault segmentation recorded by low-temperature thermochronology: Livingstone fault scarp, Malawi Rift, East African Rift System. Earth and Planetary Science Letters, 455, pp.62-72.

Olsen, K.H. and Morgan, P., 2006. Introduction: progress in understanding continental rifts. In Developments in Geotectonics (Vol. 25, pp. 3-26). Elsevier.

Perron, J.T. and Royden, L., 2013. An integral approach to bedrock river profile analysis. Earth Surface Processes and Landforms, 38(6), pp.570-576.

Pickford, M., Senut, B., Ambrosi, J.P., Dechamps, R., Faure, M., Van Damme, D., Texier, P.J., Baguma, Z. and Musiime, E., 1992. Rvision de la biostratigraphie du Nogne du Rift Occidental (Ouganda-Zare). Comptes rendus de l'Acadmie des sciences. Srie 2, Mcanique, Physique, Chimie, Sciences de l'univers, Sciences de la Terre, 315(10), pp.1289-1292.

Ring, U., 2008. Extreme uplift of the Rwenzori Mountains in the East African Rift, Uganda: Structural framework and possible role of glaciations. Tectonics, 27(4).

Roberts, E.M., Stevens, N.J., O'Connor, P.M., Dirks, P.H.G.M., Gottfried, M.D., Clyde, W.C., Armstrong, R.A., Kemp, A.I.S. and Hemming, S., 2012. Initiation of the western branch of the East African Rift coeval with the eastern branch. Nature Geoscience, 5(4), pp.289-294.

Roller, S., Wittmann, H., Kastowski, M. and Hinderer, M., 2012. Erosion of the Rwenzori Mountains, East African Rift, from in situ-produced cosmogenic10Be. Journal of Geophysical Research: Earth Surface, 117(F3).

Rosenbaum, G., Lister, G.S. and Duboz, C., 2002. Relative motions of Africa, Iberia and Europe during Alpine orogeny. Tectonophysics, 359(1-2), pp.117-129.

Rosendahl, B.R., 1987. Architecture of continental rifts with special reference to East Africa. Annual Review of Earth and Planetary Sciences, 15(1), pp.445-503.

Russell, J.M., Cohen, A.S., Johnson, T.C. and Scholz, C.A., 2012. Scientific drilling in the East African Rift Lakes: A strategic planning workshop. Sci Drill, 14, pp.49-54.

Sachau, T., Koehn, D. and Passchier, C., 2013. Mountain-building under extension. American Journal of Science, 313(4), pp.326-344.

Schneider, S., Hornung, J., Hinderer, M. and Garzanti, E., 2016. Petrography and geochemistry of modern river sediments in an equatorial environment (Rwenzori Mountains and Albertine rift, Uganda)—Implications for weathering and provenance. Sedimentary Geology, 336, pp.106-119.

Schwanghart, W. and Scherler, D., 2014. TopoToolbox 2–MATLAB-based software for topographic analysis and modeling in Earth surface sciences. Earth Surface Dynamics, 2(1), pp.1-7.

Stamps, D.S., Calais, E., Saria, E., Hartnady, C., Nocquet, J.M., Ebinger, C.J. and Fernandes, R.M., 2008. A kinematic model for the East African Rift. Geophysical Research Letters, 35(5).

Stankiewicz, J. and de Wit, M.J., 2006. A proposed drainage evolution model for Central Africa—Did the Congo flow east?. Journal of African Earth Sciences, 44(1), pp.75-84.

Underwood, C.J., King, C. and Steurbaut, E., 2013. Eocene initiation of Nile drainage due to East African uplift. Palaeogeography, Palaeoclimatology, Palaeoecology, 392, pp.138-145.

Van der Beek, P., Mbede, E., Andriessen, P. and Delvaux, D., 1998. Denudation history of the Malawi and Rukwa Rift flanks (East African Rift System) from apatite fission track thermochronology. Journal of African Earth Sciences, 26(3), pp.363-385.

Van Wijk, J.W. and Blackman, D.K., 2005. Dynamics of continental rift propagation: the end-member modes. Earth and Planetary Science Letters, 229(3-4), pp.247-258.

Wallner, H. and Schmeling, H., 2010. Rift induced delamination of mantle lithosphere and crustal uplift: a new mechanism for explaining Rwenzori Mountains' extreme elevation?. International Journal of Earth Sciences, 99(7), pp.1511-1524.

Wildman, M., Brown, R., Beucher, R., Persano, C., Stuart, F., Gallagher, K., Schwanethal, J. and Carter, A., 2016. The chronology and tectonic style of landscape evolution along the elevated Atlantic continental margin of South Africa resolved by joint apatite fission track and (U-Th-Sm)/He thermochronology. Tectonics, 35(3), pp.511-545.

Willett, S.D., McCoy, S.W., Perron, J.T., Goren, L. and Chen, C.Y., 2014. Dynamic reorganization of river basins. Science, 343(6175), p.1248765.